Raman Spectroscopy of sp^2 Nano-Carbons

Authors: Mildred S. Dresselhaus[1], G. Dresselhaus[2] and Ado Jorio[3]

Affiliations:

[1]*Department of Electrical Engineering and Physics*

Massachusetts Institute of Technology (MIT)

Cambridge, MA 02139-4307, USA

[2]*Francis Bitter Magnet Laboratory*

Massachusetts Institute of Technology (MIT)

Cambridge, MA 02139-4307, USA

[3]*Departamento de Física, Universidade Federal de Minas*

Gerais, Belo Horizonte - MG, 30123-970 Brazil

and

Divisão de Metrologia de Materiais, Instituto Nacional de Metrologia, Normalização e

Qualidade Industrial, Duque de Caxias, RJ, 25250-020, Brazil.

31 October 2008

1. Introduction

Different from scanning probe and electron microscopy-related techniques, optics is one of the oldest characterization techniques for materials science, being largely used long before nanoscience could even be imagined. In the age of nano, optics still sustains its kingdom. The advantages of optics for nanoscience relate to both experimental and fundamental aspects. Experimentally, the techniques are readily available, relatively simple to perform, possible at room temperature and under ambient pressure, and require relatively simple or no sample preparation. Fundamentally, the optical techniques (normally using infrared and visible wavelengths) are non-destructive and non-invasive because they use the photon, a massless and chargeless particle, as a probe.

The sp^2 carbon materials and Raman spectroscopy have a special place in the nanoworld. It is possible to observe Raman scattering from one single sheet of sp^2-hybridized carbon atoms, the two-dimensional (2D) graphene sheet, and from a narrow strip of graphene sheet rolled-up into a 1 nm-diameter cylinder, the one-dimensional (1D) single-wall carbon nanotube. These observations are possible just by shining light on the nanostructure focused through a regular microscope. This article focuses on both the basic concepts of sp^2 carbon nano-materials and Raman spectroscopy, together with their interaction.

1.1 Nanoscience, nanotechnology and sp^2 carbon

To fully understand the importance of Raman spectroscopy of sp^2 carbons in the nano-carbon context, it is important to understand that nano-carbons are part of the

nanoworld and address structures with sizes between the molecular and the macroscopic. The Technical Committee (TC-229) for nanotechnologies standardization of the International Organization for Standardization (ISO) defines the field of nanotechnologies as including either or both of the following:

- Understanding and control of matter and processes at the nanoscale, typically, but not exclusively, below 100 nanometers in one or more dimensions where the onset of size-dependent phenomena usually enables novel applications;
- Utilizing the properties of nanoscale materials that differ from the properties of individual atoms, molecules, and bulk matter, to create improved materials, devices, and systems that exploit these new properties.

In this sense, the integrated circuit represents the first human example of nano-technology, and gave birth to the information age. Together with the nonstop shrinking of electronic circuits, the rapid development of molecular biology and the evolution of chemistry from atoms and molecules to large complexes, such as proteins and quantum dots, have launched nanotechnology. It is not possible to clearly envisage the future results of nanotechnology, or even the limit for the potential of nanomaterials, but clearly serious fundamental challenges have to be overcome:

- To construct nanoscale building blocks precisely and reproducibly;
- To find and to control the rules for assembling these objects into complex systems;
- To predict and to probe the emergent properties of these systems.

These challenges are not only technological, but also conceptual: how to treat a system that is too big to be solved by present day first principles calculations, and too small for statistical methods? Although these challenges punctuate nanoscience and

nanotechnology, the success here will represent a revolution in larger-scale scientific challenges in the fields of emergent phenomena and information technology. The answers to questions like ``how do complex phenomena emerge from simple ingredients?" and ``how will the information technology revolution be extended?" will probably come from nanotechnology.

It is exactly in this context that nano-carbon is playing a very important role. From one side, nature shows that it is possible to manipulate matter and energy the way integrated circuits manipulate electrons, by assembling complex self-replicating carbon-based structures able to sustain life. From another side, carbon is the upstairs neighbor to silicon in the periodic table, with more flexible bonding and unique physical, chemical and biological properties, which nevertheless hold promise of a revolution in electronics at some future time. Three important aspect make sp^2 carbon materials special for facing the nano-challenges listed in the previous paragraph: First the unusually strong covalent bonding between neighboring atoms, second the extended π-electron clouds, and third the simplicity of the system. We elaborate shortly about those aspects in the following paragraphs.

Carbon has six electrons, two are core 1s states, and four occupying the 2s and 2p orbitals. In the sp^2 configuration, the 2s, p_x and p_y orbitals mix to form three covalent bonds, 120^o from each other in the xy plane (see Fig.1). Each carbon atom has three neighbors, forming a hexagonal network. These sp^2 bonds are stronger than the sp^3 bonding in diamond, making graphene (a single sheet of sp^2 atoms) stronger than diamond in tensile strength. This added strength is advantageous for sp^2 carbons as a prototype material for the development of nanoscience and nanotechnology, since

different interesting nanostructures (sheets, ribbons, tubes, horns, fullerenes, etc.) are stable and strong enough for exposure to many different types of characterization and processing steps.

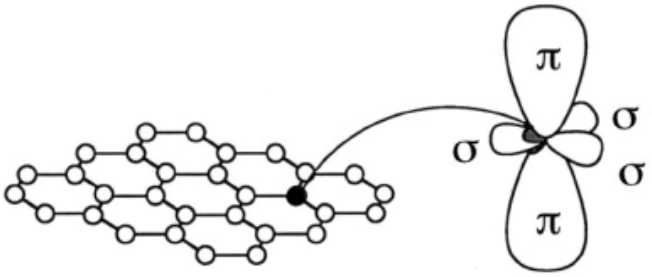

Fig.1. The carbon atomic orbitals in the sp^2 honeycomb lattice. (Charlier, 2008)

The p_z electrons that remain perpendicular to the hexagonal network (see Fig.1) form the delocalized π electron states. For this reason, sp^2 carbons, which includes graphene, graphite, carbon nanotubes, fullerenes and other carbonaceous materials, are also called π-electron materials. These delocalized electronic states are highly unusual, because they behave like relativistic Dirac Fermions, i.e. exhibit a massless-like linear momentum-energy relation (like a photon), and are responsible for unique optical and transport (both thermal and electronic) properties.

These two properties accompany a very important aspect of sp^2 carbons, the simplicity of a system formed by only one type of atom in a periodic hexagonal structure. Therefore, different from most materials, sp^2 nano-carbons allow us to access their special properties from both experimental and theoretical approaches. Being able to model the structure is crucial for the development of our methodologies and knowledge.

1.2. The importance of graphite, carbon nanotubes and graphene

The ideal concept of sp^2 nano-carbons starts with the graphene sheet (see Fig.2). Add one, two layers and you have the bi-, tri-layer graphene. Roll-up a narrow strip of graphene into a seamless cylinder and you have a single-wall carbon nanotube (SWNT). Add one-, two-layer concentric cylinders and you have double-, triple-wall carbon nanotubes. Many rolled-up cylinders would make a multi-wall carbon nanotube (MWNT), and many flat layers give graphite. This ideal concept is didactic, but historically these materials came to human knowledge in the opposite order.

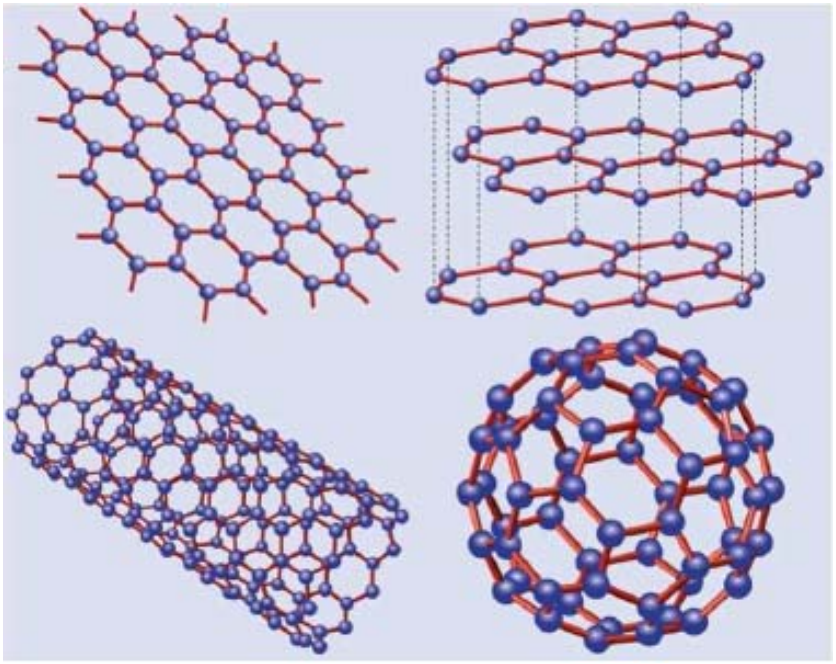

Fig.2. The sp^2 carbon materials, including single-layer graphene (top-left), triple-layer graphene (top-right), single-wall carbon nanotube (bottom-left) and a C_{60} fullerene, which included pentagons in the structure (bottom-right). (Castro-Neto 1998).

Three-dimensional (3D) graphite is one of the longest-known forms of pure carbon, formed by graphene planes usually in an ABAB stacking (Wykoff 1981). Of all materials, graphite has the highest melting point (4200 K), the highest thermal

conductivity (3000 W/mK) and a high room temperature electron mobility (30,000 cm^2/Vs) (Dresselhaus 2008). Graphite and its related carbon fibers (Dresselhaus 1988) have been used commercially for decades. Their applications range from use as conductive fillers and mechanical structural reinforcements in composites (e.g., in the aerospace industry) to their use in electrode materials utilizing their resiliency (e.g., in batteries) (Endo 2008).

In 1985 a unique discovery in another sp^2 carbon system took place, the C_{60} fullerene molecule (see Fig.2) (Kroto 1985). The fullerenes stimulated and motivated a large scientific community from the time of its discovery up to the end of the century, but their applications remain sparse to date. Carbon nanotubes arrived on the scene following the footsteps of the C_{60} fullerene molecule. Carbon nanotubes have evolved into one of the most intensively studied materials, and are held responsible for co-triggering the nanotechnology revolution.

The big rush on carbon nanotube science started after the observation of multi-wall carbon nanotubes (MWNTs) on the cathode of a carbon arc used to produce fullerenes (Iijima 1991), even though they were identified in the core structure of vapor grown carbon fibers as very small carbon fibers in the 1970s (Oberlin 1976) and in the 1950s in the Russian literature (Radushkevich 1952) (see Fig.3). Single-wall carbon nanotubes (SWNTs) where first synthesized in 1993 (Iijima 1993, Bethume 1993). The interest in the fundamental properties of carbon nanotubes and their exploitation through a wide range of applications is due to their unique structural, chemical, mechanical, thermal, optical, optoelectronic and electronic properties (Saito 1998, Reich 2003). The growth of a single SWNT at a specific location and pointing in a given direction (Zhang 2001,

Huang 2003), and the growth of a huge amount of millimeter-long tubes with nearly 100 % purity (Hata 2004) have been achieved (Joselevich 2008). Substantial success with the separation of nanotubes (Arnold 2006) by metallicity and length has been achieved and advances have been made with doping nanotubes for the modification of their properties (Terrones 2008). Studies on nanotube optics, magnetic properties, transport and electrochemistry have exploded, revealing many rich and complex fundamental excitonic and other collective phenomena (Jorio 2008). Quantum transport phenomena, including quantum information, spintronics and superconducting effects have also been explored (Biercuk 2008). After a decade and a half of intense activity in carbon-nanotube research, more and more attention is now focusing on the practical applications of the many unique and special properties of carbon nanotubes (Endo 2008).

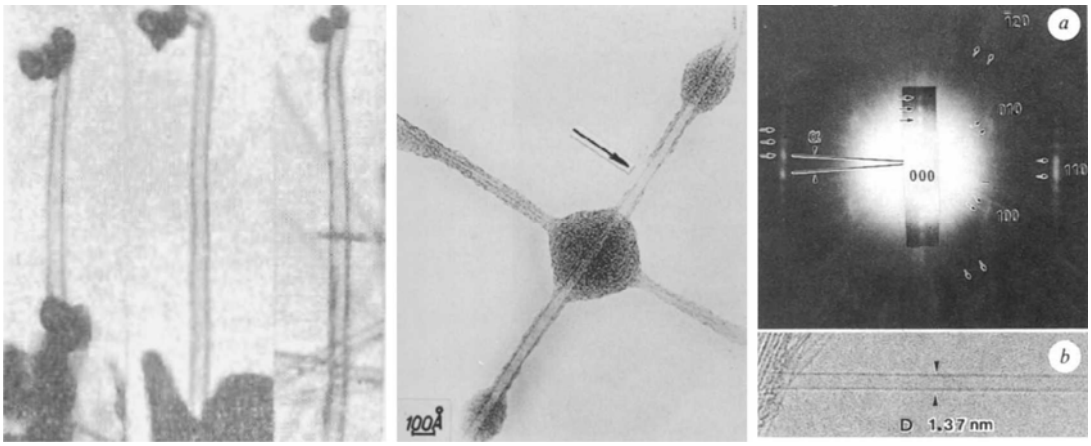

Fig.3. The transmission electron microscopy images of carbon nanotubes. The early reported observations in 1952(a) (Radushkevich 1952) and 1976 (a) (Oberlin 1976) and the observation of single-walled carbon nanotubes that launched the field in 1993 (b) (Iijima 1993)

In the mean time, the study of nano-graphite was under development, and in 2004, Novoselov et al. discovered a simple method to transfer a single atomic layer of carbon from the c-face of graphite to a substrate suitable for the measurement of its electrical and optical properties (Novoselov 2004). This finding led to a renewed interest in what was considered to be a prototypical, yet theoretical, two-dimensional system, providing a basis for the structure of graphite, fullerenes, carbon nanotubes and other nano-carbons. Surprisingly, this very basic graphene system, which had been studied for many decades, suddenly appeared with many novel physical properties that were not even imagined previously (Geim 2007, Castron-Neto 2008). In one or two years, the rush on graphene science started. The scientific interest was stimulated by the report of the relativistic properties of the conduction electrons (and holes) in a single graphene layer less than 1 nm thick, that is responsible for the unusual properties in this system (see Fig.4) (Zhang 2005, Novoselov 2005). Many groups are now making devices using graphene and also graphene ribbons which have a long length and a small width, and where the ribbon edges play an important role.

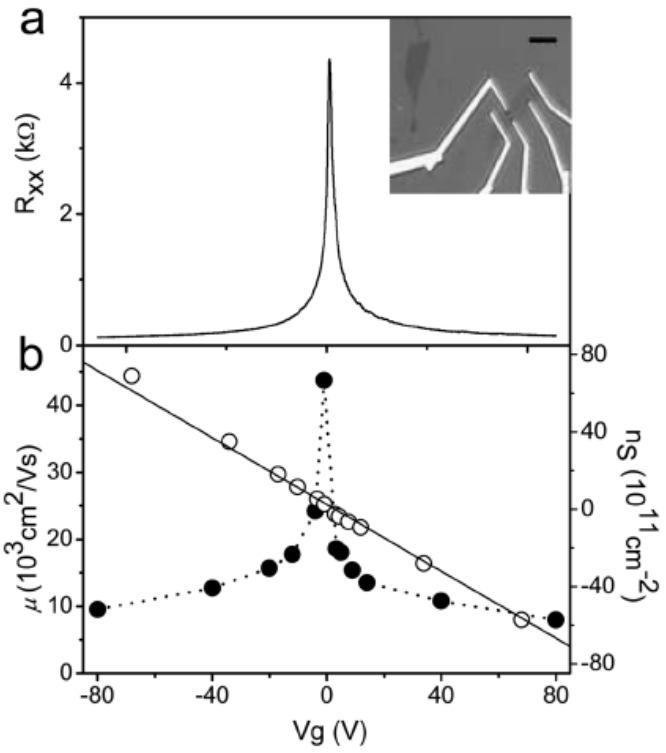

Fig.4. Resistivity, mobility and carrier density as a function of gate voltage V_g (Vg in the figure) in a single-layer graphene field effect transistor device (Charlier 2008). (a) V_g-dependent R_{xx} showing a finite value at the Dirac point, where the valence and conduction bands are degenerate and the carriers are massless. The resistivity ρ_{xx} can be calculated from R_{xx} using the geometry of the device. The inset is an image of a graphene device on a Si:SiO_2 substrate. The Si is the bottom gate; five top electrodes formed via e-beam lithography are shown in the inset. The scale bar is 5 μm. (b) Mobility μ and carrier density n_s as a function of V_g (for holes $V_g < 0$ and for electrons $V_g > 0$). The mobility (dotted curve) diverges at the Dirac point due to the finite resistivity. (Zhang 2005).

Having introduced nano-carbons in the nanoworld, we now focus on the Raman spectroscopy of nano-carbons. Section 2 gives the basic concepts of light-matter interaction and Raman spectroscopy. A more detailed presentation of state-of-the-art

Raman spectroscopy of sp^2 nano-carbons is given in section 3, followed by a critical discussion in section 4. Section 5 summarizes the main aspects of this paper, and section 6 presents future perspectives.

2. Background

2.1 Light-matter interaction and Raman spectroscopy

When shining light into a material, part of the energy can just pass through (transmission), while the remaining energy interacts with the system through several different mechanisms (see Fig.5). From the light that interacts with the system, many different effects might occur: (i) a photon, which is the quantum unit of light, can be absorbed and transformed into atomic vibrations, i.e. heat, which can be represented by phonons, the quantum units of lattice vibrations; (ii) a photon can be absorbed and transformed into a photon with a lower energy that is emitted. This process is called photoluminescence and it happens in semiconducting materials when the energy of the incident photon exceeds the energy gap between the valence and conduction bands; (iii) a photon may not be absorbed, but it just shakes the electrons, which will scatter that energy back into another photon with the same energy as the incident one. This is an elastic scattering process and it is named Rayleigh scattering; (iv) the photon may shake the electrons, causing oscillations of the atoms according to their natural vibrational frequencies, thereby changing the electronic configuration of the atoms. In this case, when the electrons scatter the energy back into another photon, this photon will have lost or gained energy to or from the atoms. This is an inelastic scattering process called Raman scattering. Many other processes may occur but they are usually less important

for the energetic balance of light-matter interaction. The amount of light that will be transmitted, as well as the details for all the light-matter interactions will be determined by the electronic and vibrational properties of the material, thus making light a very powerful characterization tool for materials science studies, while gentling perturbing the material.

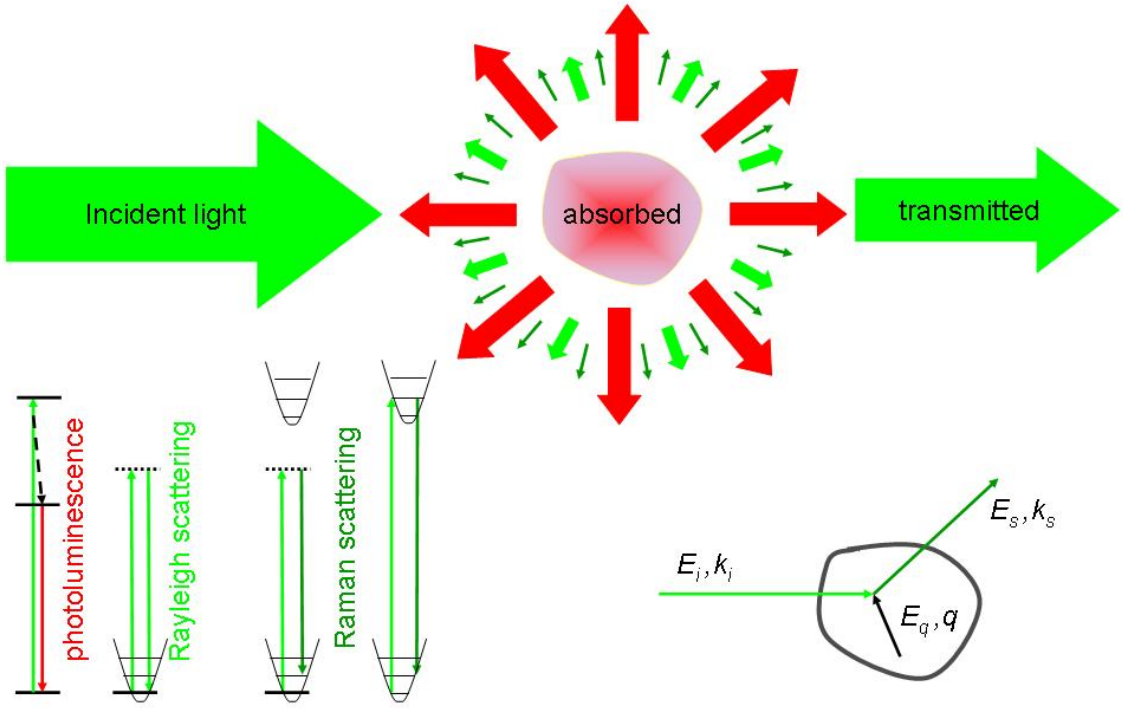

Fig.5. The light-matter interaction, showing the most usual processes, with energy balance displayed in the bottom left. The vertical arrows indicate the electron excitation (up) and emission (down). The dashed lines indicate virtual electronic states in the elastic (Rayleigh) and non-resonant inelastic (Raman) scattering processes. Vertical lines indicate the different vibrational levels inside an electronic level (parabola). The diagram on the bottom-right stands for the Raman process, and it defines the energy and momentum of the incident (E_i, k_i) and scattered (E_S, k_S) light, as well as the phonon (E_q, q) that is emitted (Stokes process) or absorbed (anti-Stokes process).

2.2 The basic concepts of Raman spectroscopy

This section gives the basic definitions for the terms that are used in describing Raman spectroscopy, and points the reader to references where detailed experimental results and theory related to each concept can be found.

2.2.1. Raman scattering

The Raman effect refers to the inelastic scattering of light. An incident photon with energy $E_i = E_{laser}$ and momentum $k_i = k_{laser}$ reaches the sample and is scattered, resulting in a photon with a different energy E_S and momentum k_S (see Fig.5). For energy and momentum conservation:

$$E_S = E_i \pm E_q, \quad (1)$$

$$K_S = k_i \pm k_q, \quad (2)$$

where E_q and k_q are the energy and momentum change during the scattering event, mediated by an excitation of the medium. Although electronic excitations can result from Raman scattering, the most usual scattering outcome is the excitation of atomic normal mode vibrations. These vibrational modes are related to the chemical and structural properties of materials, and since every material has a unique set of such normal modes, Raman spectroscopy can be used to probe materials properties in detail and to provide an accurate characterization of specific materials. Raman spectroscopy in particular provides a rich variety of characterization information regarding carbon nanostructures.

2.2.2 Stokes and anti-Stokes Raman processes

In the inelastic scattering process, the incident photon can decrease or increase its energy by creating (Stokes) or destroying (anti-Stokes) a quantum of normal mode vibration (i.e. a phonon) in the medium. The plus (minus) signs in Eqs.1 and 2 apply when energy has been received from (transferred to) the medium. The probability for the two types of events depends on the excitation photon energy E_i, and this dependence can be explored for an accurate determination of electronic transition energies. Furthermore, the probability to destroy a phonon depends on the phonon population given by the Bose-Einstein distribution and, consequently, the anti-Stokes event depends also on the temperature, according to:

$$I_S/I_{AS} = [(E_i - E_q)/(E_i + E_q)]^3 \exp(E_q/kT), \quad (3)$$

where I_S and I_{AS} denote the measured intensity for the Stokes and anti-Stokes peaks, respectively, k is the Boltzmann constant and T is the temperature. Because the anti-Stokes process is usually less probable than the Stokes process, it is usual that people only care about the Stokes spectra. In this work, when not referring explicitly to the type of process, it is the Stokes process that is being addressed.

2.2.3. Energy conservation

A Raman spectrum is a plot of the scattering intensity as a function of $E_S - E_{laser}$. Therefore, the energy conservation relation given by Eq.1 is the most important aspect of Raman spectroscopy. Although the anti-Stokes process has a positive net energy, it is the Stokes spectra that is most usually measured, and for simplicity the Stokes process is designated as being positive. The Raman spectra will show peaks at $\pm E_q$, where E_q is the energy of the excitation associated with the Raman effect. The quantum of

excitation denoting the normal vibrational modes is named the phonon, and it is regularly used to describe the lattice vibrations in crystals. We will use the term "phonon" frequently in this article. The phonon excitation energies are found by decomposing the atomic vibrations into the vibrational normal modes of the material.

2.2.4. Energy units

The energy axis in the Raman spectra is usually displayed in units of cm^{-1}. Lasers are usually described by the wavelength of the light, i.e. in nanometers, but the phonon energies are usually too small a number when displayed in nm, which is not a comfortable unit for denoting Raman shifts. The accuracy of a common Raman spectrometer is on the order of 1 cm^{-1}, which is equivalent to 10^{-7}nm. The energy conversion factors are: 1 eV = 8065.5 cm^{-1} = 2.418×10^{14} Hz = 11,600 K. Also 1 eV corresponds to a wavelength of 1.2398 μm.

2.2.5. Shape of the Raman peak

The response of a forced damped harmonic oscillator, in the limit that the peak frequency ω_q is much larger than the peak width Γ_q, is a Lorentzian curve. Therefore, the Raman peaks usually have a Lorentzian shape. The center of the Lorentzian gives the natural vibration frequency, and the full width at half maximum (FWHM) is related to the damping, which gives the phonon lifetime. However, in specific cases the Raman feature can deviate from the simple Lorentzian shape. One obvious case is when the feature is actually composed by many phonon contributions. Then the Raman peak will be a convolution of several Lorentzian peaks, giving rise to Gaussian, Voigt or more complex lineshapes. Another case is when the lattice vibration couples to electrons. In this case additional line broadening and even an asymmetric lineshape can result. These

effects are observed in certain metallic sp^2 carbon materials and are discussed on a theoretical basis in (Dresselhaus 2005).

2.2.6 Resonance Raman Effect

The laser energies are usually much higher than the phonon energies. Therefore, although the exchange in energy between light and the medium is transferred to the atomic vibrations, the light-matter interaction is mediated by electrons. Usually the photon energy is not large enough to achieve a real electronic transition, and the electron that absorbs the light is said to be excited to a "virtual state", from where it couples to the lattice, generating the Raman scattering (see Fig. 5). However, when the excitation laser energy matches the energy gap between the valence and conduction bands in a semiconducting medium (or between an occupied initial state and an unoccupied final state more generally), the probability for the scattering event to occur increases by many orders of magnitude, and the process is then called a resonance Raman process (non-resonant otherwise). The same happens if the scattered light matches such an electronic transition. The resonance effect is extremely important in systems where electronic transitions are in the visible range, which includes sp^2 carbon systems.

2.2.7. First and higher-order Raman processes

The order of the Raman process is given by the number of phonons involved in the scattering. The most usual case is the first-order Stokes Raman scattering process, where the photon energy exchange creates one phonon in the medium with a very small momentum ($q \approx 0$). If 2, 3 or more phonons are involved in the same scattering event,

the process is a second, third, or higher-order, respectively. The first-order Raman process gives the basic quanta of vibration, while higher-order processes give very interesting information about harmonics and combination modes. More information on this topic can be found in (Dresselhaus 2005)

2.2.8 Vibrational Structure

Describing the vibrations of small molecules is simple. The number of vibrational modes is given by the number of degrees of freedom for atomic motion (i.e. the number of atoms N multiplied by 3 dimensions, minus 6, the six coming from translations along x, y, z and rotations around these axes). The number of vibrational energy levels may be smaller than 3N-6 since some levels can be energy degenerate. Finding the normal modes of large and complex molecules, such as proteins, is not an easy task, and in cases like that vibrations are usually grouped and labelled by their local bondings (e.g., C-C, C=C, C=O, etc.). Crystals have a large number of atoms (ideally infinite), but periodic systems are, again, quite simple to describe, although such descriptions require an understanding of the *phonon dispersion relations*.

Since ideal crystalline structures have an infinite number of atoms, the number of vibrational levels is infinite. The vibrational structures of these systems are displayed in a plot of the phonon energy (ω_q) vs. phonon wavevector q, i.e. the phonon dispersion relation for each distinct normal mode phonon. The ω_q vs. q plots are composed of continuous curves called phonon branches. Being continuous, they account for the infinity of vibrational levels. The number of phonon branches depends on the number of degrees of freedom for the atomic motion for a unit cell for this material. The

wavevector q is defined by the magnitude and phase for a normal mode vibration that can involve more than one consecutive unit cell.

2.2.9. Momentum conservation and back-scattering

The q vector carries information about the wavelength of the vibration ($q = 2\pi/\lambda$) and the direction along which the oscillation occurs. For $\lambda \rightarrow \infty$, then we have $q \rightarrow 0$, and we usually denote the center of the phonon dispersion relation as the Γ point. The phonon wavelength λ cannot be smaller than the unit cell vector $\boldsymbol{a}$, which defines an upper limit for the relevant values of q, namely, the unit cell of the crystal in reciprocal space, which is called the first Brilluoin zone, and this zone provides a bounding polygon that confines the phonon dispersion. For $q > | \pm \pi/a|$, the phonon structure will repeat itself.

The momentum conservation given by eq.2 is illustrated in Fig. 5. Different scattering geometries are possible, and specific choices may be used to select different phonons due to symmetry selection rules (Dresselhaus 2005). The back-scattering configuration, for which k_i and k_s have the same direction and opposite signs, is the most common when working with nanomaterials, because a microscope is usually needed to focus the light onto small samples. Furthermore, in the first-order Raman process, the momentum transfer is usually neglected, i.e. $k_S - k_i \sim 0$. Phonon momentum $k_S \neq 0$ become important in defect-induced or higher-order Raman scattering processes, and the theoretical background for such processes can be found in (Saito 2003).

This discussion gives the idea on why the first-order Raman process can only access phonons at $q \rightarrow 0$, i.e. at the Γ point. The momenta associated with the first-order light scattering process are on the order of $k_i = 2\pi/\lambda_{light}$, where λ_{light} is in the visible range (800-400 nm). Therefore, k_i is a very small number when compared to the dimensions of the first Brillouin zone, which is limited to vectors no longer than $q = 2\pi/a$, where the unit cell vector $\boldsymbol{a}$ in real space is on the order of tenths of nm.

2.2.10 Coherence

It is not trivial to define whether a real system is big enough to be considered as effectively infinite and to exhibit a quasi-continuous phonon (or electron) energy dispersion relation. Whether or not a dispersion relation can be defined indeed depends on the process that is under evaluation. In the Raman process, how long does it take for an electron excited by the incident photon to decay? Considering this scattering time, what is the distance felt by an electron? These problems are described in solid state physics textbooks by the concept of coherence. The coherence time is the time the electron takes to suffer an event such as scattering that changes its state. Thus, the coherence length is the size over which the electron maintains its integrity, its coherence, and it is defined by the electron speed and the coherence time which can be measured experimentally. The Raman process is an extremely fast process, in the range of femto-seconds (10^{-15} s). Considering the speed of electrons in graphite (10^6 m/s), this gives a coherence length on the order of nm. Interestingly this number is much smaller than the wavelength of visible light. Actually, this is a particle picture for the scattering process and playing with these concepts is actually quite interesting.

3. Presentation of state-of-the-art Raman spectroscopy of sp^2 nano-carbons

Figure 6 shows the Raman spectra from different crystalline and disordered sp^2 carbon nanostructures. The first-order Raman bands go up to 1620 cm^{-1}, and the spectra above this value is composed of overtone and combination modes. We focus here on the Raman spectra from crystalline structures (sections 3.1-3.4) and on the disorder caused by defects in the sp^2 structure (section 3.5). The bottom spectrum in Fig. 6 is from amorphous carbon that exhibits a considerable amount of sp^3 bonds and some hydrogen satisfying dangling bonds. This is a rich field with important applications for industry, but outside the scope of this article. Discussions on amorphous carbon can be found in (Ferrari 2004).

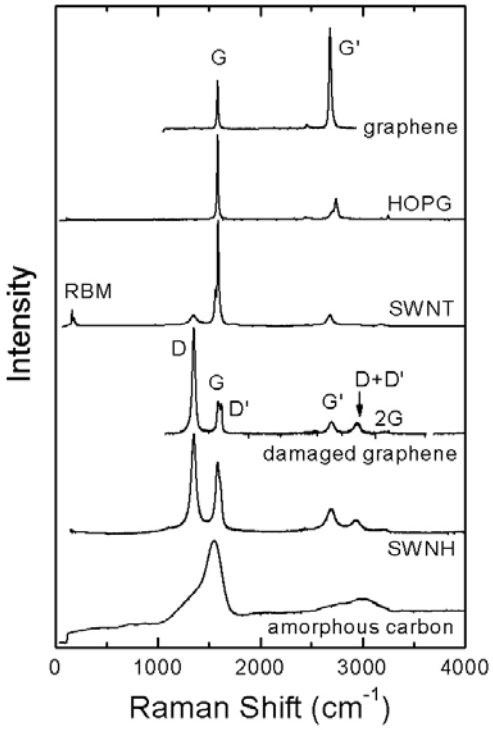

Fig.6: Raman spectra from several sp^2 nano-carbons. From top to bottom: crystalline graphene, highly oriented pyrolytic graphite (HOPG), single-wall carbon nanotube (SWNT) bundles, damaged graphene, single-wall carbon nanohorns (SWNH) and

hydrogenated amorphous carbon. The most intense Raman peaks are labeled in a few spectra.

3.1 The sp^2 model system: graphene

Among the sp^2 carbon systems, monolayer graphene is the simplest and has, consequently, the simplest Raman spectra (see Fig.7). The ideal graphene is a two-dimensional crystalline sheet, one atom thick, with two C atoms in a unit cell that repeats itself to infinity. Its Raman spectra is marked by two strong features, named the G and G′ bands (G from graphite), as discussed below.

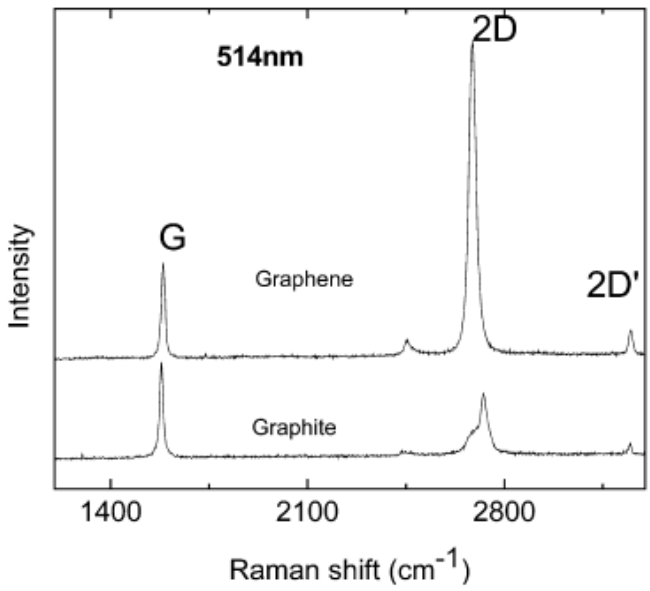

Fig.7: Raman spectrum of single-layer graphene and graphite. The two most intense features are the first-order Raman allowed G band and the second-order G′ band (labeled 2D in the figure making reference to its origin as a second-order process related to the disorder induced D peak). The spectrum of pristine single-layer graphene is unique in sp^2 carbons for exhibiting a very intense G′ band as compared to the G band (Ferrari 2006, Charlier 2008).

3.1.1. The G band

The most usual Raman peak observed in the Raman spectra of any sp^2 carbon system has historically been baptized the G band. The G mode is related to the stretching of the bonds between the nearest neighbor A and B carbon atoms in the unit cell. This feature appears around 1585 cm^{-1} (see Fig. 7), but exhibits some specificities according to the particular nano-carbon sp^2 system under discussion and according to ambient conditions of temperature, pressure, doping and disorder. Because of the peculiar electronic dispersion of graphene, being a zero gap semiconductor with a linear E(*k*) dispersion relation, the G band phonons (energy of 0.2 eV) can promote electrons from the valence to the conduction band. For this reason, the electon-phonon coupling in this system is quite strong, and gives rise to a renormalization of the electronic and phonon energies, including a sensitive dependence on electron or hole doping (Das 2008). The full width at half maximum (FWHM) intensity observed for graphene on top of a Si/SiO_2 substrate usually ranges from 6 to 16 cm^{-1}, depending on the graphene to substrate interactions.

Furthermore, interesting confinement and polarization effects can be observed in the G band of a graphene nanoribbon, as shown by (Cancado 2004). The G_1 band from the nanoribbon on top of an HOPG substrate can be separated from the substrate G_2 band by use of laser heating (see Fig.8). The temperature rise of the ribbon due to laser heating is greater than that of the substrate and ω_{G1} for the ribbon decreases more than for the substrate because of the higher thermal conductivity of the substrate relative to the graphene ribbon. The ribbon G_1 band shows a clear antenna effect, where the Raman signal disappears when crossing the light polarization direction with respect to the ribbon axis, in accordance with theoretical predictions (Dresselhaus 2005).

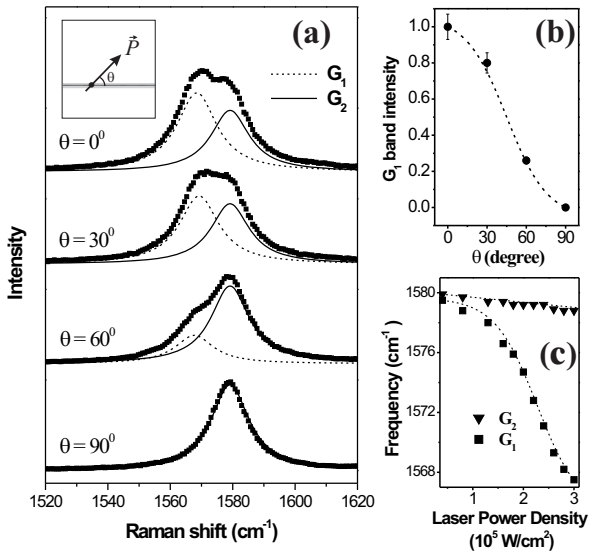

Fig.8. (a) The G band Raman spectra from the graphene nanoribbon (G_1) and from the graphite substrate (G_2). (b) The G_1 dependence on the light polarization direction with respect to the ribbon axis including experimental points and theoretical predictions in the dashed curve. (c) Frequency of the G peaks as a function of incident laser power for the graphene ribbon (G_2) and the HOPG substrate (G_1). (Cancado 2004).

3.1.2. The G` band

The second most usual Raman peak observed in the Raman spectra of any sp^2 carbon system has been historically baptized as the G` band. It is a second-order peak involving two phonons with opposite wavevectors q and $-q$, the atomic motion related to the phonon looking like a breathing of the hexagon rings. This feature appears at around 2700 cm^{-1} (see Fig. 7) for laser excitation energy of 2.41 eV (514 nm), while the highest phonon frequency in graphene is around 1620 cm^{-1}. The scattering by the related one-phonon process is not allowed by symmetry and has been baptized as the D-band, denoting the dominant disorder-induced band (see section 3.5.1). Besides a rich dependence of the G` band on the ambient conditions (temperature, pressure, doping),

this band exhibits a very interesting resonance phenomena related to the laser excitation energy. By increasing (decreasing) E_{laser}, the G` peak frequency $\omega_{G`}$ will increase (decrease), as is also the case of the D band at $\omega_D \approx \omega_{G`}/2 \approx 1350$ cm^{-1} for $E_{laser} = 2.41$ eV (see section 3.5.3).

3.2 Adding graphene layers: from single layer graphene to graphite

When increasing the number of graphene layers from one to two, 2 atoms are added to the unit cell (see Fig. 9), thus increasing the number of phonon branches. Here we consider tri-layer graphene as having an ABA Bernal stacking, like highly oriented pyrolytic graphite (HOPG). Rhombohedral graphite has ABC stacking, but it will not be considered here (Wickoff 1981). We now discuss the main changes in the Raman spectra when adding layers to the graphene system, i.e. bi-layer, tri-layer, many-layer (graphite).

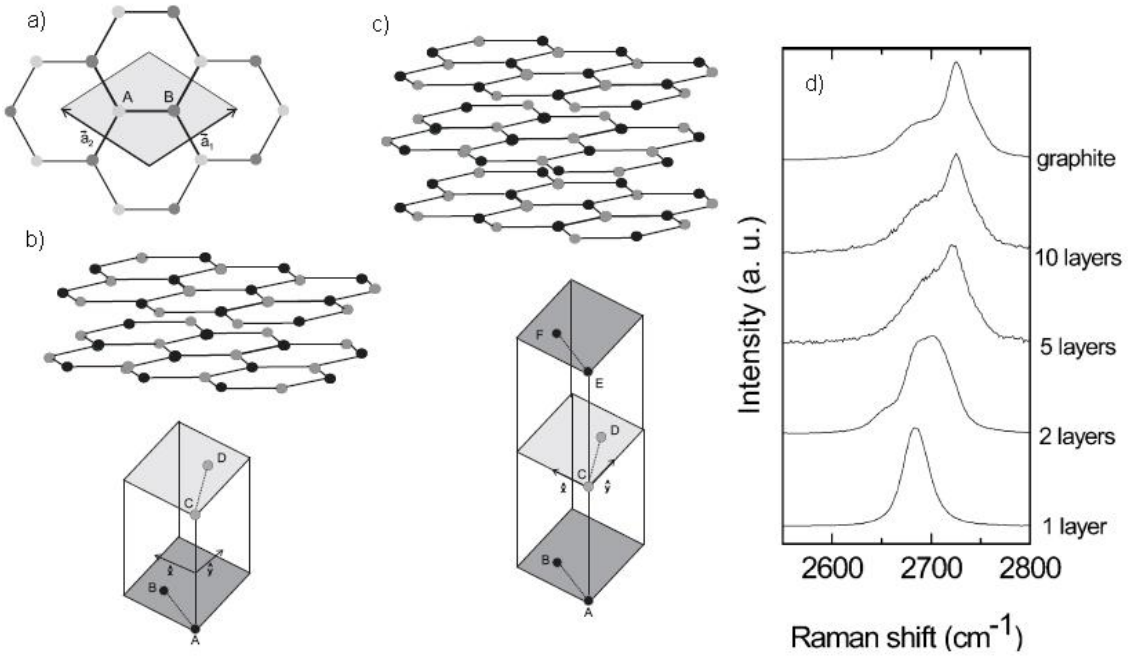

Fig.9. Schematics for mono- (a), bi- (b) and tri- (c) layers graphene (Malard 2008). (d) Evolution of the G′ band spectra at 514 nm (E_{laser} = 2.41 eV) with the number of graphene layers. (Ferrari 2006, Charlier 2008)

3.2.1. The G` band

While the first-order G band spectrum is approximately independent of the number of layers, the G` spectrum shows the most characteristic changes and for this reason the G` band can be used to determine the number of layers (Ferrari 2006) and the stacking order (Pimenta 2007, Ni 2008) of few layer graphene. The G` spectrum from single layer graphene has one peak, while from bi-layer graphene with AB stacking order, 4 distinct peaks can be observed (see Fig.9(d)). If the double layer has no stacking order, there is a small upshift in frequency, but only one peak is observed (Ni 2008). The number of peaks increases with increasing number of layers. However, it is not possible to clearly distinguish all of these peaks since the splitting among them is not larger than their linewidths. Thus for graphite (the limit of a semi-infinite number of layers), the G` band is found to contain only two well-defined peaks when the out-of-plane AB stacking is perfect. Turbostratic graphite (no stacking order) has, again, a one peak G` band lineshape (Pimenta 2007).

3.2.2. Other Raman features

Other features are usually observed in graphite, and are identified as combination modes and overtones (others than the G` band). Examples are the features observed above 2000 cm^{-1} in Fig. 6. The mode assignment upon which these features are based is discussed in

(Dresselhaus 2005). Furthermore, many other Raman features are observed when disorder is present in nano-carbons, as discussed in section 3.5.

3.3. Rolling up one graphene layer: the single-wall carbon nanotube (SWNT)

The single wall carbon nanotube (SWNT) can be obtained by rolling up a strip of graphene into a cylinder (see Fig. 10). This procedure can generate tubes with different diameters (d_t), by changing the width of the graphene strip, and different chiral angles (θ), by changing the angle between the carbon bonds and the tube axis. These two characteristic parameters (d_t,θ) define the SWNT structure, and are usually represented by the (*n,m*) indices, which describe the number of $\mathbf{a_1}$ and $\mathbf{a_2}$ graphene lattice vectors needed to build the so called chiral vector $\mathbf{C_h} = n\mathbf{a_1} + m\mathbf{a_2}$. The chiral vector $\mathbf{C_h}$ spans the circumference of the tube cylinder (see Fig. 10).

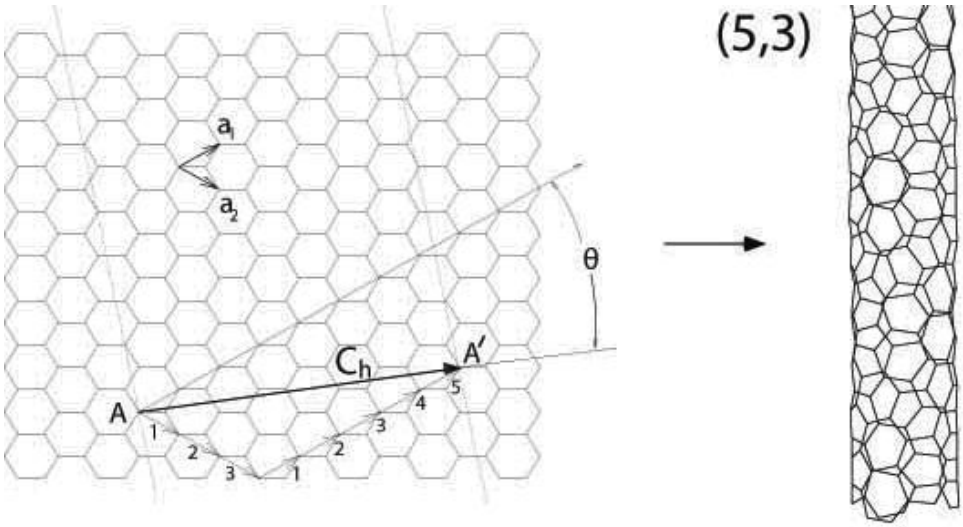

Fig.10: Schematic diagram showing a possible rolling up of a strip of two-dimensional graphene sheet into a tubular form. In this example, a (5,3) nanotube is under construction and the resulting tube is illustrated on the right (Saito 1998).

Of course rolling up a graphene strip is an idealized picture. The carbon nanotubes are actually formed by carbon atoms in the vapor phase self-organizing themselves to form a tube structure when growing from a nanometer size catalyst particle. Different growth methods generate samples with very different aspects, like isolated tubes on different substrates or suspended tubes over trenches, tubes in bundles, tubes (isolated or in bundles) that are aligned along a specific direction. Furthermore, tube processing can generate samples in different environments, such as liquids or wrapped by DNA molecules (Joselevich 2008).

The most spectacular differences when comparing SWNT and graphene are observed due to quantum confinement effects, which are also completely different from the effects on graphite ribbons due to satisfying the carbon bond requirements at the edges of the ribbon. As a very simple example, the zero-energy translation of the graphene generates, when rolling it up into a tube, the so-called radial breathing mode, discussed in section 3.3.1 below. Furthermore, due to the spatial confinement in this one-dimensional system, their optical properties are discrete, like for molecules. The physics behind it is related to the formation of spikes, named van Hove singularities, in the density of electronic states (Saito 1998, Dresselhaus 2005) and the formation of excitons (bounded electron-hole pairs) for the optical transitions, as is discussed in (Dresselhaus 2006). These van Hove singularities and the exciton formation generates an absorption picture for SWNTs that, although very rich in different phenomena (Dresselhaus 2006), is mostly dominated by strong discrete optical transition levels, usually denoted by E_{ii} , where i = 1,2,3... enumerates the optical transition energy levels (Saito 1998, Dresselhaus 2005). The E_{ii} optical trantision energies depend on (d_t,θ), or

alternatively on (*n,m*), and many of them lie in the visible range, thus generating strong resonance Raman effects, as discussed in the following sections.

3.3.1. The radial breathing mode (RBM)

The radial breathing mode (RBM) Raman feature corresponds to the coherent vibration of all the C atoms of the SWNT in the radial direction, as if the tube were "breathing". This feature is unique to carbon nanotubes and occurs with frequencies ω_{RBM} typically between 110 and 350 cm^{-1} for SWNTs for diameters in the range 0.7 nm < d_t < 2 nm. These RBM frequencies are therefore very useful for identifying whether a given carbon material contains SWNTs, through the presence of the Raman-active RBM modes (see Fig. 6). When the excitation laser energy is in resonance with the optical transition energy E_{ii} from one isolated SWNT, its RBM can be seen, as shown in the left panel of Fig. 11. The (*n,m*) assignment can be made based on the RBM measurement, as discussed in the next section. The natural linewidth (FWHM) for isolated SWNTs on a SiO_2 substrate is $\Gamma = 3$ cm^{-1} (Dresselhaus 2005), but much narrower linewidths (down to ~ 0.25 cm^{-1}) have been observed for the inner tubes of double wall carbon nanotubes (DWNTs) at low temperatures (Pfeiffer 2008).

The RBM gives the nanotube diameter through use of the relation $\omega_{RBM} = (227/d_t)(1+C/d_t^2)^{1/2}$. Therefore, from the ω_{RBM} measurement of an individual isolated SWNT (see left panel in Fig.11), it is possible to obtain its d_t value. The parameter 227 cm^{-1}nm has been obtained experimentally for a single type of sample (Araujo 2008), and it is in agreement with theoretical predictions based on the elastic constant of graphite (Mahan 2002). Most of the samples, however, exhibit an upshift in ω_{RBM} (see

Fig. 11) due to tube-environment van-der Waals type interactions, and this interaction can be taken into account by making the parameter $C \neq 0$ for each specific sample (Araujo 2008). The RBM spectra for SWNT bundles contain RBM contributions from different SWNTs in resonance with the laser excitation line (see Fig.11), and a careful spectral analysis gives the tube diameter distribution in the bundles.

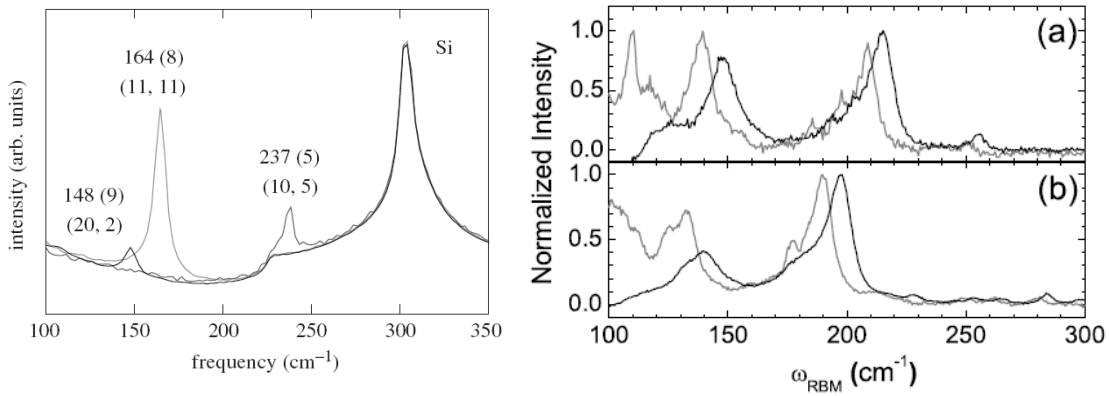

Fig.11. (left panel) Raman spectra of a Si/Si_2 substrate containing isolated SWNTs grown by the CVD method (Jorio 2001). The spectra are taken at three different spots on the substrate where the RBM Raman signal from resonant SWNTs are found. The RBM frequencies (linewidths) are displayed in cm^{-1}. Also shown are the (*n,m*) indices assigned from the Raman spectra for each resonant tube. The step at 225 cm^{-1} and the peak at 303 cm^{-1} come from the Si/SiO_2 substrate. (right panel) The RBM Raman spectra for "super-growth" SWNTs (gray) and for "alcohol CVD" SWNTs (black). The samples are different and exhibit different E_{ii} resonance values. The four spectra are obtained using different excitation laser lines: (a) 590nm (gray) and 600nm (black); (b) 636nm (gray) and 650nm (black), so that in (a) and (b) the same (*n,m*) SWNTs are in resonance. The gray and black spectra are shifted from each other due to the different environments seen by the SWNTs in the two types of samples. (Araujo 2008)

3.3.2. The resonance Raman effect in the RBM and the (*n,m*) assignment

When the excitation laser energy matches one of the discrete optical transition energies E_{ii} for a given SWNT, there is large enhancement in the Raman intensity (resonance Raman effect). Therefore, for interpreting the Raman spectra of SWNTs, a very useful guide is the so-called Kataura plot, where the transition energies E_{ii} are plotted as a function of nanotube diameter d_t (see left panel in Fig.12). Such a plot can be directly related to the RBM spectra (see right panel in Fig.12).

If resonance with a single tube is achieved ($E_{laser} = E_{ii}$) and its RBM is observed, it is possible to assign its specific (*n,m*), since (E_{ii},ω_{RBM}) can be related to (d_t,θ) (Jorio 2001). For a more general diameter characterization of a bundled SWNT sample based on the RBMs, it is necessary to work with the Kataura plot (Dresselhaus 2005). A single Raman measurement gives the RBM for the specific tubes that are in resonance with that laser line, which may not give a complete characterization of the diameter distribution of the sample. By taking the Raman spectra with many excitation laser lines, a good characterization of the diameter distribution in the sample can be obtained (Dresselhaus 2005, Araujo 2007). Since semiconducting (S) and metallic (M) tubes of similar diameters do not occur at similar E_{ii} values, ω_{RBM} measurements using several laser energies E_{laser} can be also used to characterize the ratio of metallic to semiconducting SWNTs in a given sample (Samsonidze 2004, Miyata 2008).

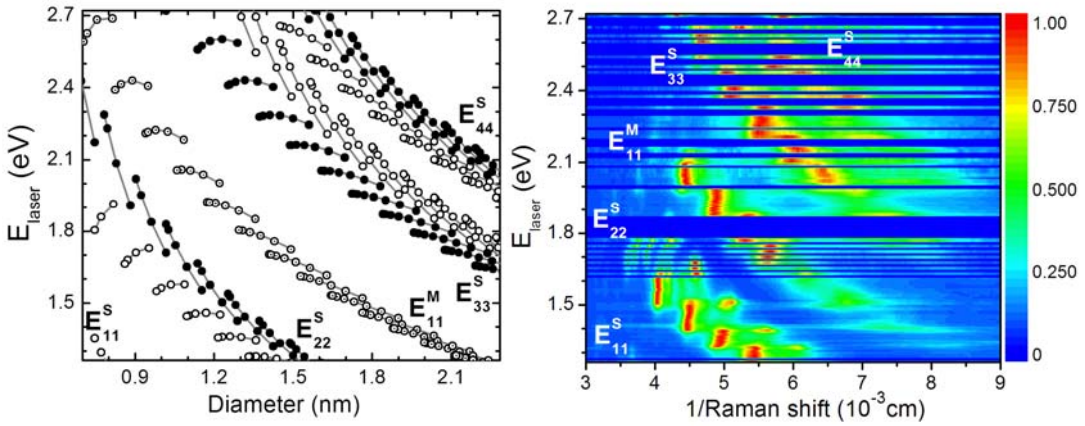

Fig.13. (left) The optical transition energies (dots) of SWNTs as a function of tube diameter (Jiang 2007a). The superscripts S and M for the E_{ii} labels indicate the optical transitions for semiconducting and metallic SWNTs, respectively. (right) 2D color map showing the SWNT RBM spectral evolution as a function of laser excitation energy. The intensity of each spectrum is normalized to the strongest peak, and we plot the RBM results in terms of the inverse Raman shift. The right and left panels show coincident axes and can be directly correlated (Araujo 2007).

A careful analysis of the resonance Raman intensities in the right panel of Fig.12 shows that the RBM intensity has a strong (*n,m*) dependence, as explained in (Jiang 2007b). This effect is mostly due to a chiral angle dependence of the electron-phonon coupling, plus a diameter dependence of the electron-radiation interaction due to excitonic effects (Jiang 2007b, Dresselhaus 2006).

3.3.3. The G band

In contrast to the graphite Raman G band, which exhibits one single Lorentzian peak at 1582 cm^{-1} related to the tangential mode vibrations of the C atoms, the SWNT G-band is composed of multi-peaks due to the phonon wave vector confinement along the SWNT circumferential direction and due to symmetry-breaking effects associated with

SWNT curvature (see Fig. 13). The G-band frequency in SWNTs can be used for: (1) diameter characterization, the lower frequency G^- peak exhibiting a frequency dependence on diameter (see Fig. 13(b,c)); (2) to distinguish between metallic and semiconducting SWNTs, through major differences in their Raman lineshapes (see Fig. 13(a)); (3) to probe the charge transfer arising from doping a SWNT (Terrones 2008); and (4) to study the selection rules in the various Raman scattering processes and scattering geometries (Dresselhaus 2005).

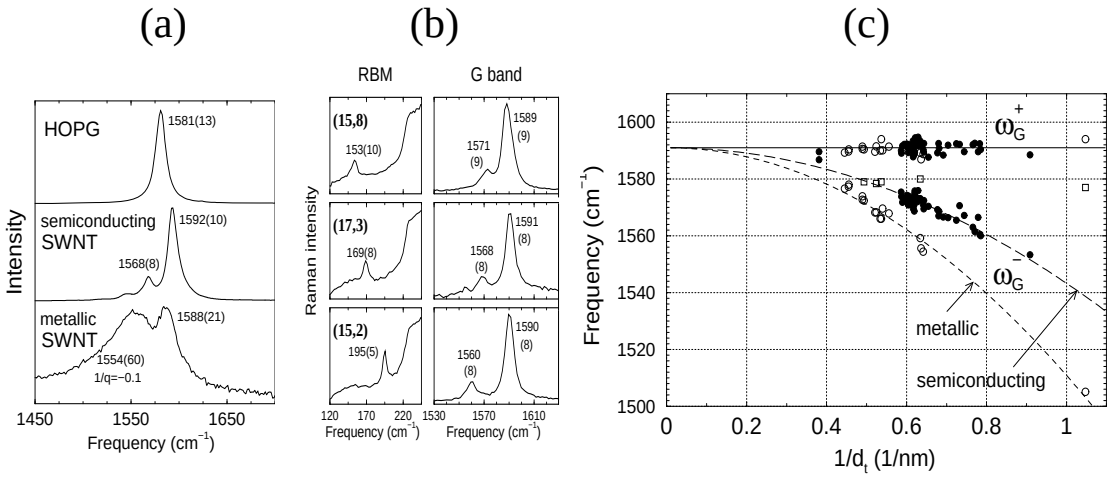

Fig.13. (a) The G-band for highly oriented pyrolytic graphite (HOPG), one semiconducting SWNT and one metallic SWNT. For C_{60} fullerenes a peak is observed at 1469 cm^{-1}, but it is not considered a G band. (b) the radial breathing mode (RBM) and G-band Raman spectra for three semiconducting isolated SWNTs of the indicated (n,m) values. (c) Frequency vs. $1/d_t$ for the two most intense G-band features (ω_G- and ω_G^+) from isolated SWNTs (Dresselhaus 2005).

Elaborating a bit more on item (2) above, the difference between the G band spectra from metal and semconducting tubes is the strong coupling between electrons and G band phonons in metals. Although up to 6 modes are Raman allowed in the G band of

SWNTs (Dresselhaus 2005), the G band is dominated by two strong peaks that can be represented by the C-C stretching along the circumferential direction or along the axis, usually named the transverse optical (TO) and longitudinal optical (LO) modes, respectively. The LO mode strongly couples to electrons in metals, being largely downshifted in frequency and broadened (see Fig. 13(a)). The physics related to this coupling has been discussed in (Piscanec 2004, Ando 2006).

3.3.4 The G` band

Like for the other sp^2 carbons, the G` Raman spectra provide unique information about the electronic structure of both semiconducting and metallic SWNTs. The G′-band sometimes appears (at the individual nanotube level) in the form of unusual two-peak structures for both semiconducting and metallic nanotubes (Samsonidze 2003, Dresselhaus 2005), even if there is no interlayer coupling, like in bi-layer graphene and graphite. The two-peak G′-band Raman features observed from semiconducting and metallic isolated nanotubes are shown in Figs.14(a) and (b), respectively. The presence of two peaks in the G`-band Raman feature from semiconducting SWNTs indicates resonance with two different vHSs of the same nanotube, occurring independently for both the incident E_{laser} and scattered E_{laser} -$E_{G'}$ photons.

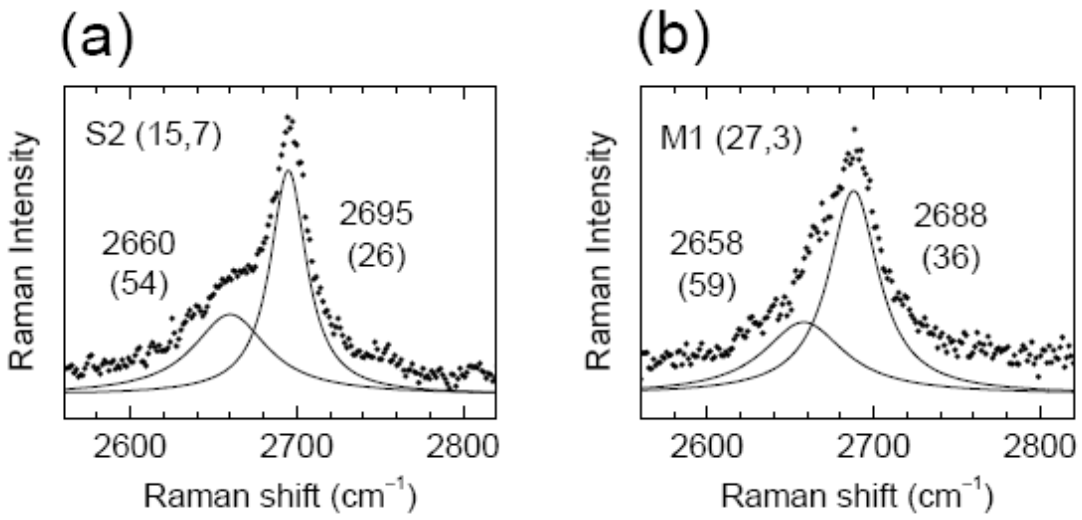

Fig.14. The *G′*-band Raman features for (a) semiconducting (15, 7) and (b) metallic (27, 3) nanotubes showing unusual two-peak structures (Samsonidze 2003).

3.3.5 Other features

Carbon nanotubes also exhibit several combination modes and overtones. Basically all the Raman features observed in graphite can also be seen in carbon nanotubes. Furthermore, carbon nanotubes exhibit several Raman features in the spectral region between 400—1200 cm^{-1}, which are called intermediate frequency modes (IFMs), since their frequencies lie between the common ω_{RBM} and ω_G modes (Dresselhaus 2005). Some of the IFMs are fixed in energy, some are "dispersive" (Raman shift changes when changing the excitation energy), and are attributed to combination modes. It is not yet clear whether these modes are related to disorder or not. Theory relates their observation with confinement along the tube length (Saito 1998), and some supporting experimental evidence has been found for such an effect (Chou 2007). However, the IFM picture is not yet fully understood.

3.4. Adding tube-layers: double- and multi-wall carbon nanotubes

The differences between single, double and many-wall carbon nanotubes are often classified by the diameter distribution in the tubes. MWNTs, for example, usually have tubes with very large diameters d_t, with inner diameters over 10 nm, and outer diameters rising up to about 100 nm. Their spectra approach that of graphite, since no confinement effects can be observed. Only general line broadening differentiates large MWNTs from graphite (see Fig.15).

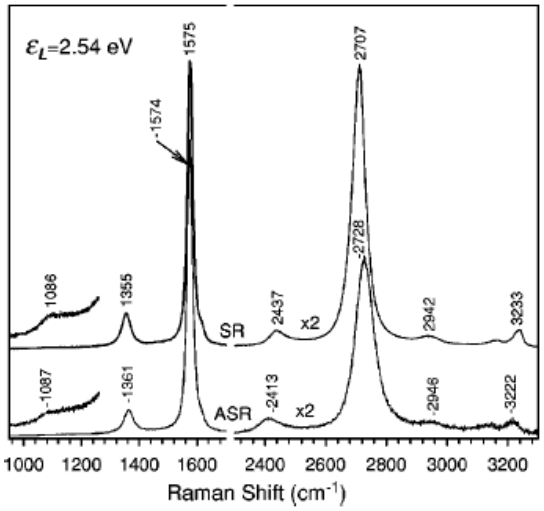

Fig.15. Stokes (SR) and anti-Stokes (ASR) Raman spectra from MWNTs (Tan 2002). The small difference in frequencies when comparing the same peak at the SR and ASR spectra are due to the double resonance effect, as discussed in detail in (Cancado 2002, Tan 2002).

For DWNTs, however, very interesting outer vs. inner tube effects have been observed. The most striking is the observation of many different ω_{RBM} for the same (*n,m*) inner SWNT, due to different possible outer tubes (see Fig. 16). Furthermore, charge transfer effects depending on metal vs. semiconducting outer vs inner configuration have been

observed (Souza Filho 2007). While most of these results have been obtained from DWNTs in bundles, measurements on isolated DWNTs are expected to be very informative (Villalpando 2008).

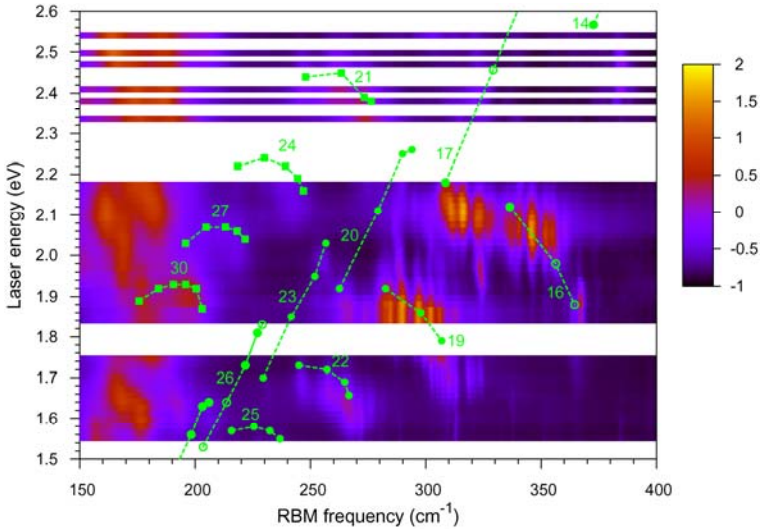

Fig.16. The 2D RBM Raman map for DWNTs. The E_{ii} points from the Kataura plot are superposed (green bullets). It is clear there are many more RBM features than (*n,m*) related E_{ii} values (Pfeiffer 2008).

3.5. Disorder in sp^2 systems

When the size of a graphite system is reduced, disorder effects start to be seen. Disorder can also be seen at defect locations or at graphene/graphite edges.

3.5.1. The D band

The so-called D band (D comes from disorder) is observed in any sp^2 carbon system when the lattice periodicity is broken by a disorder mechanism, such as defects. This feature appears around 1350 cm^{-1} (for E_{laser} = 2.41 eV) and the phonon-related step of the D band double resonance process corresponds to one of the steps in the G` band

process. The D band itself is a second-order process in which the elastic scattering of the defect allows for momentum conservation in the phonon creation, and the defect breaks the Raman scattering selection rules. The D band has been largely used to characterize disorder in carbon materials (see Fig.17). The D band is dispersive, like the G′ band, and shows interesting phenomena in SWNTs due to electron and phonon confinement (Dresselhaus 2005, Pimenta 2007).

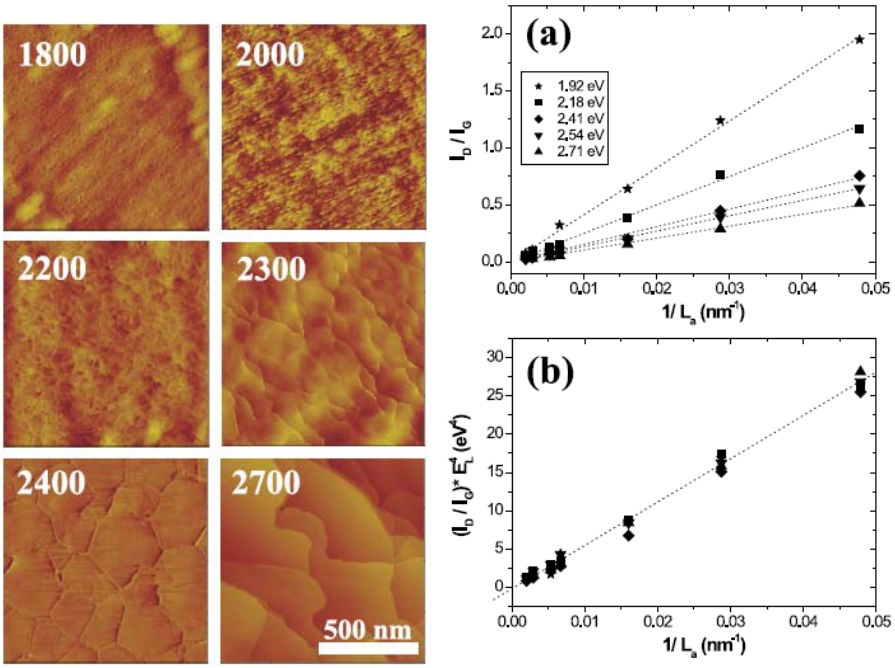

Fig.17. (left panels) STM images of graphite crystallites. The crystallite size L_a varies with the annealing temperature in ^oC (displayed in the images). (right panels) The evolution of the D/G intensity ratio (I_D/I_G) as a function of crystallite size (a) for different laser excitation energies. (b) All the curves in (a) collapse into one curve when considering the dependence of the G band intensity on the fourth power of the incident laser excitation energy, E_{laser}^4 (Pimenta 2007).

3.5.2. The D` band

The so-called D` band, appearing around 1620 cm^{-1}, is another feature commonly observed in many of the sp^2 disordered carbon systems. This feature is usually much weaker than the D band, and for this reason the D band is more often used for disorder characterization. Whereas the D band is connected with an intervalley scattering process from the K to the K′ points, in the Brillouin zone, the D′ band is connected with an intravalley scattering process around the K point or around the K′ point. The D and D′ bands tend to be sensitive to defects of different physical origin, but these differences require further study.

3.5.3. The G` band

The G` band is not disorder induced but it can be used to study changes in the electronic and vibrational structure related to disorder. The 2D vs. 3D stacking order of graphene layers is one example. Highly crystalline 3D graphite shows two G′ peaks (see the top spectra of Fig.9(d)). When the interlayer stacking order is lost, a one-peak feature starts to develop, identified with 2D graphite, and the peak is centered near the middle of the two peaks in the G′ lineshape from ordered graphite (Pimenta 2007).

Furthermore, localized emission of a red-shifted G′ band was observed and related to the local distortion of the nanotube lattice by a negatively charged defect. The opposite occurs for *p* doping and this effect can be used to study SWNT doping (see Fig. 18) (Maciel 2008).

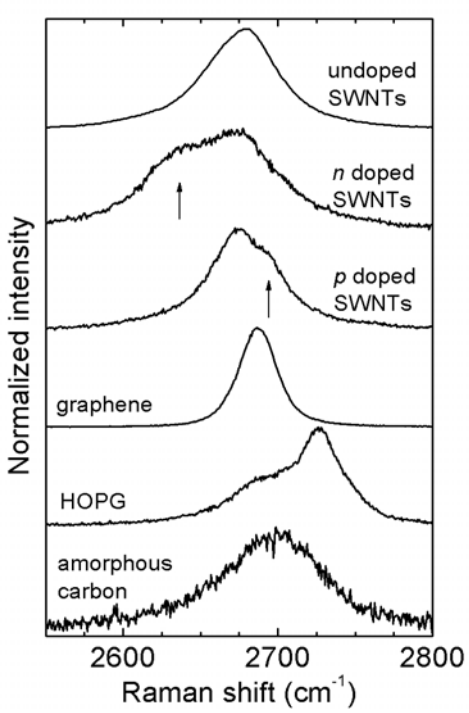

Fig.18. The *G*' Raman band in different sp^2 carbon materials measured at room temperature with E_{laser} = 2.41 eV (514 nm). The arrows point to defect-induced peaks in the G′ band for doped SWNTs. The *p*/*n* doping comes from substitutional boron/nitrogen atoms (Terrones 2008), the nearest neighbors of carbon in the periodic table. The spectra of graphene, HOPG and amorphous carbon are shown for comparison. (Maciel 2008).

3.6. Other Raman modes and other sp^2 carbon structures

In general the observation of overtones and combination modes in condensed matter systems is rare because of dispersion effects which make these features too weak and broad to pick out from the noisy background. The double resonance process (Saito 2003), however, allows such overtones and combination modes to be quite clearly observed (Dresselhaus 2005), thereby providing new information about SWNT

properties. Nanowiskers, nanobuds, nanorods, nanohorns exhibit a large number of peaks (see Fig.18), always related to and assignable from the phonon structure of graphene.

Although we do not cover fullerenes here, when talking about overtones it is specially interesting to mention their Raman spectra. As a molecular carbon structure, a fullerene has an specially rich overtone spectra which can be seen in both Raman and infrared spectra. A detailed discussion on this topic can be found in (Dresselhaus 1996).

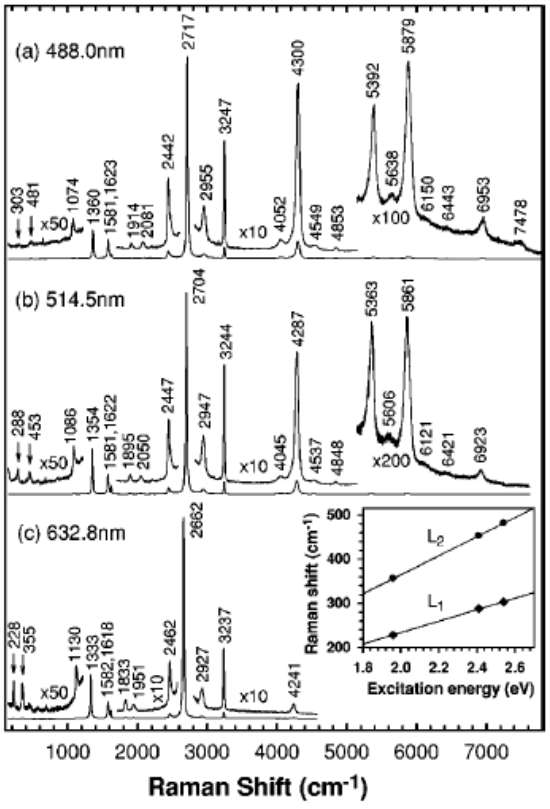

Fig. 18. Raman spectra of graphite wiskers obtained with three different laser excitation lines (Tan 2002, Ferrari 2004). Note that some phonon frequencies vary with E_{laser}, some do not. The inset to (c) show details of some peaks that are dispersive, and are explained theoretically by the double-resonance effect (Saito 2003).

4. Critical Discussions

As discussed in section 3, Resonance Raman spectroscopy (RRS) was shown to provide a powerful metrological tool for distinguishing among the different sp^2 nano-carbons, the number of layers of a graphene sample, the AB stacking order in many-layers graphene of graphite, the metallic (M) from semiconducting (S) tubes, for determining the diameter distribution of SWNTs in a given sample, for determining the (*n,m*) values for specific tubes, the doping and many other important properties. Recent RRS measurements done on the E^S_{22}, E^M_{11}, E^S_{33}, E^S_{44}, E^M_{22}, E^S_{55} and E^S_{66} transitions on water assisted CVD grown SWNTs (Araujo 2008) suggest that tubes in the interior of the forest of aligned SWNTs seem to be well shielded from environmental effects and may provide a standard reference material for SWNTs that show minimal environmental effects. This suggestion needs further experimental confirmation, but if this interpretation is correct, such a reference material might represent the first nano-carbon standard reference material, which could be useful for quantitative determinations of environmental effects in nanotubes. Such effects are important for understanding current nanotube photo-physics studies where samples routinely experience environmental effects due to substrates, wrapping agents, functionalization, strain or molecules adsorbed in suspended nanotubes, and similar problems also arise for graphene and the other nano-carbons. Controlling environmental effects are vital for a variety of uses of nano-carbons for sensors and biomedical applications.

Calculations of Raman frequencies and RRS matrix elements are now at an advanced stage for SWNTs, but understanding lifetime effects, dark singlet and triplet states are still incomplete. The characterization of MWNTs (multiwall carbon nanotubes) as well

as many layers graphene by RRS is at an early stage, though a good start has been made on the characterization of DWNTs (double wall carbon nanotubes) and bi-layer graphene which are, respectively, the simplest examples of a MWNT or of graphite. The effect of edge states in graphene is expected to be a rich field and it is basically until now unexplored by spectroscopy.

5. Summary

In summary, we presented here the basic concepts for Raman spectroscopy and the Raman signatures of sp^2 carbon materials. The G band at ~1585 cm^{-1} has a single-Loretzian peak structure for 2D and 3D materials, and shows a special lineshape for their one-dimensional counterparts, carbon nanotubes, with a doublet rather than a single Lorentzian feature. Raman spectroscopy can also be used to differentiate between metallic and semiconducting carbon nanotubes, as well as to obtain information on tube diameter and the tube diameter distribution of a bundled sample. Another important feature is the G` band which appears at ~2700 cm^{-1} for 2.41 eV (514 nm) excitation. This feature is highly sensitive to the electronic structure, changing shape when comparing single, bi-, tri-layer graphene, stack-ordered (3D) graphite and pyrolytic (2D) graphite and when nano-carbons are doped. The cylindrical carbon nanotubes are the only nano-carbon material showing the low frequency radial breathing modes which are, strongly dependent on diameter, and usually appear in the range 50-350 cm^{-1}. Finally, at ~1350 cm^{-1} ($\approx \omega_{G'}/2$) the D peak can be observed when there is disorder in the material, i.e. any perturbation that breaks the sp^2 periodic structure, and the D-band can be used for characterizing the structural quality of carbon-based materials. Finally, many other features related to disorder, overtone and combination modes are observed,

most of them being weak, but sometimes they are strong. Although the assignment and frequency behavior has been quite well understood, the variation in intensity of these features still remain an open issue.

6. Future Perspectives

It is clear the Raman spectroscopy of sp^2 carbons remains a fruitful field of research even though many advances have already been achieved. A big step forward in the field will occur when Raman spectroscopy starts to be combined in a single instrument with microscopy techniques, either high resolution electron transmission microscopy (HRTEM) or scanning probe microscopies, like atomic force microscopy (AFM) or scanning tunneling spectroscocpy (STM). Combining the information from real space (microscopy) with information from momentum space (spectroscopy) should bring in new insights, including new understanding of different types of disorder. In this context, near-field studies should also bring in important new understanding, since Raman spectroscopy with spatial resolution down to 10nm can be achieved, providing important information on the science of defects (Hartschuh 2003, Maciel 2008).

Furthermore, there is now a major focus devoted to directing the nano-carbon field to applications, which urges studies on metrology, standardization and industrial quality control (Jorio 2007, Jorio 2008b). The development of protocols for the definition of sample parameters like structural metrics (carbon-carbon distance, surface area, tube diameter, chiral angle, ribbon width), physical properties (optical, thermal, mechanical), composition (impurity content, spatial homogeneity) and stability (dispersability, bio-compatibility and health effects) are important for both research and applications of

nano-carbons. These metrological protocols are expected to be applicable not only to nano-carbon materials, but also to the exploding field of nano-materials, where metrology issues will drive technological growth and innovation. Nanoscience promises a revolution in technology, bringing us back to the very basic problem of defining metrics and measurement systems, and ultimately back to the fundamentals needed for advancing the metrology for samples of nanoscale size, for which the properties, measurement systems and metrological approaches differ from those for bulk systems. That is to say, the characterization of a sample 1 μm in size and another sample 1 nm in size will require different measurement strategies, because in the nano-scale regime, the length scale itself becomes a parameter describing the properties of a material.

7. References

(Ando 2006) Ando, T., 2006. Anomaly of Optical Phonon in Monolayer Graphene. *J. Phys. Soc. Jpn.* 75: 124701

(Araujo 2007) Araujo, P. T., Doorn, S. K., Kilina, S., Tretiak, S., Einarsson, E., Maruyama, S., Chacham, H., Pimenta, M. A., Jorio, A. 2007. Third and Fourth Optical Transitions in Semiconducting Carbon Nanotubes. *Phys. Rev. Lett.* 98: 067401

(Araujo 2008) Araujo, P. T., Maciel I. O., Pesce, P. B. C., Pimenta, M. A., Doorn, S. K., Qian, H.,. Hartschuh, A, Steiner, M, Grigorian, L.,Hata, K., and Jorio, A., 2008. Nature of the constant factor in the relation between radial breathing mode frequency and tube diameter for single-wall carbon nanotubes. *Phys. Rev. B* 77: 241403(R)

(Arnold 2006) Arnold, M.S., Green, A. A., Hulvat, J. F., Stupp, S. I., Hersam, M. C. 2006. Sorting carbon nanotubes by electronic structure using density differentiation. *Nature Nanotechnol.* 1: 60–65

(Bethume 1993) Bethune, D. S., Kiang, C. H., deVries, M. S., Gorman, G., Savoy, R., Vazquez, J., Beyers R., 1993. Cobalt catalysed growth of carbon nanotubes with single atomic layer wells. *Nature* 363: 605–607

(Biercuk 2008) Biercuk, M. J., Ilani, S., Marcus, C. M., McEuen, P. L., 2008. Electrical Transport in Single-Wall Carbon Nanotubes. In *Carbon Nanotubes: Advanced Topics in the Synthesis, Structure, Properties and Applications*, ed. A. Jorio, M. S. Dresselhaus, and G. Dresselhaus, 63-100. Springer Series in Topics in Appl. Phys. Vol. 111.

(Cancado 2002) Cancado, L. G., Pimenta, M. A., Saito, R., Jorio, A., Ladeira, L. O., Grueneis, A., Souza-Filho, A. G., Dresselhaus, G., Dresselhaus, M. S. 2002. Stokes and anti-Stokes double resonance Raman scattering in two-dimensional graphite. *Phys. Rev. B* 66: 035415

(Cancado 2004) Cancado, L. G. Pimenta, M. A., Neves, B. R. A., Medeiros-Ribeiro, G., Enoki, T., Kobayashi, Y., Takai, K., Fukui, K., Dresselhaus, M. S., Saito, R., Jorio, A. 2004. Anisotropy of the Raman Spectra of Nanographite Ribbons. *Phys. Rev. Lett.* 93: 047403

(Castro-Neto 2008) Castro Neto, A. H., Guinea, F., Peres, N. M. R., Novoselov, K. S., Geim, A. K. 2008. The electronic properties of graphene. arXiv:0709.1163V2

(Charlier 2008) Charlier, J.-C.,. Eklund, P.C, Zhu, J., Ferrari, A.C., 2008. Electron and phonon properties of graphene: Their relationship with Carbon nanotubes. In *Carbon Nanotubes: Advanced Topics in the Synthesis, Structure, Properties and Applications*, ed. A. Jorio, M. S. Dresselhaus, and G. Dresselhaus, 673-708. Springer Series in Topics in Appl. Phys. Vol. 111.

(Chou 2007) Chou, S. G., Son, H., Zheng, M., Saito, R., Jorio, A., Kong, J., Dresselhaus, G., Dresselhaus, M. S., 2007. Finite length effects in DNA-wrapped carbon nanotubes. *Chem. Phys. Lett.* 443: 328-332

(Das 2008) Das, A., Pisana, S., Charkraborty, B., Piscanec, S., Saha, S. K., Waghmare, U. V., Novoselov, K. S., Krishnamurthy, H. R., Geim, A. K., Ferrari, A. C. & Sood, A. C., 2008. Monitoring dopants by Raman scattering in an electrochemically top-gated graphene transistor. *Nature Nanotech*. 3: 210-215.

(Dresselhaus 1988) Dresselhaus, M. S. Dresselhaus, G. Sugihara, K. Spain, I. L. Goldberg, H. A., 1988. Graphite Fibers and Filaments. Springer Series in Materials Science, Springer-Verlag, Berlin. Vol.5

(Dresselhaus 1996) Dresselhaus, M. S., Dresselhaus, G., Eklund, P., 1996. Science of Fullerenes and Carbon Nanotubes. Academic Press, New York.

(Dresselhaus 2005) Dresselhaus, M. S., Dresselhaus, G., Saito. R., Jorio, A., 2005. Raman spectroscopy of Carbon Nanotubes. *Phys. Rep.* 409: 47-99.

(Dresselhaus 2006) Dresselhaus, M. S., Dresselhaus, G., Saito, R., Jorio, A., 2006 Exciton Photophysics of Carbon Nanotubes. *Ann. Rev. Phys. Chem.* 58: 719-47

(Endo 2008) Endo, M., Strano, M. S., Ajayan, P. M., 2008. Potential Applications of Carbon Nanotubes. In *Carbon Nanotubes: Advanced Topics in the Synthesis, Structure, Properties and Applications*, ed. A. Jorio, M. S. Dresselhaus, and G. Dresselhaus, 13-61. Springer Series in Topics in Appl. Phys. Vol. 111.

(Ferrari 2004) Ferrari, A. C. Robertson, J., 2004. Raman spectroscopy in carbons: From nanotubes to diamond. *Phil. Trans. R. Soc. Lond. A* 362: 2267-2565

(Ferrari 2006) Ferrari, A. C., Meyer, J. C., Scardaci, V., Casiraghi, C., Lazzeri, M., Mauri, F., Piscanec, S., Jiang, D., Novoselov, K. S., Roth, S. Geim, A. K., 2006. Raman Spectrum of Graphene and Graphene Layers. *Phys. Rev. Lett.* 97: 187401.

(Geim 2007) Geim, A. K., Novoselov, K. S., 2007. The rise of graphene. *Nat. Mat.* 6(3):183-191

(Hartschuh 2003) Hartschuh, A., Sanchez, E. J., Xie, X. S., Novotny, L., 2003. High-resolution near-field Raman microscopy of single-walled carbon nanotubes, *Phys. Rev. Lett.* 90: 095503–095506

(Hata 2004) Hata, K., Futaba, D. N., Mizuno, K., Namai, T., Yumura, M. Iijima S., 2004. Water-assisted highly efficient synthesis of impurity-free single-walled carbon nanotubes, *Science* 306: 1362–1364

(Huang 2003) Huang, S. M., Cai, X. Y., Liu, J., 2003. Growth of millimeter-long and horizontally aligned single-walled carbon nanotubes on flat substrates. *J. Am. Chem. Soc.* 125: 5636–5637

(Iijima 1991) Iijima, S., 1991. Helical microtubules of graphitic carbon, *Nature* 354: 56.

(Iijima 1993) Iijima, S., Ichihashi, T.: Single shell carbon nanotubes of 1-nm diameter, Nature **363**, 603–605 (1993)

(Jiang 2007a) Jiang, J., Saito, R., Samsonidze, Ge. G., Jorio, A., Chou, S. G., Dresselhaus, G., Dresselhaus, M. S., 2007. Chirality dependence of exciton effects in single-wall carbon nanotubes: Tight-binding model. Phys. Rev. B 75: 035407.

(Jiang 2007b) Jiang, J., Saito, R., Sato, K., Park, J. S., Samsonidze, Ge. G., Jorio, A., Dresselhaus, G., Dresselhaus, M. S., 2007. Exciton-photon, exciton-phonon matrix elements, and resonant Raman intensity of single-wall carbon nanotubes. *Phys. Rev. B* 75: 035405.

(Jorio 2001) Jorio, A., Saito, R., Hafner, J. H., Lieber, C. M., Hunter, M., McClure, T., Dresselhaus, G., Dresselhaus, M. S., 2001 Structural (n,m) determination of isolated single-wall carbon nanotubes by resonant Raman scattering, *Phys. Rev. Lett.* 86: 1118–1121

(Jorio 2007) Jorio, A., Dresselhaus, M. S., 2007. Nanometrology Links State-of-the-Art Academic Research and Ultimate Industry Needs for Technological Innovation. MRS Bull. 34(12): 988-993.

(Jorio 2008a) Jorio, A. , Dresselhaus, M. S. & Dresselhaus, G., 2008. *Carbon Nanotubes: Advanced Topics in the Synthesis, Structure, Properties and Applications*. Springer Series in Topics in Appl. Phys. Vol. 111.

(Jorio 2008b) Jorio, A., Kauppinen, E., Hassanien, A., 2008. Carbon-Nanotube Metrology. In *Carbon Nanotubes: Advanced Topics in the Synthesis, Structure, Properties and Applications*, ed. A. Jorio, Dresselhaus, M. S., and G. Dresselhaus, 63-100. Springer Series in Topics in Appl. Phys. Vol. 111.

(Joselevich 2008) Joselevich, E., Dai, H., Liu, J., Hata, K., 2008. Carbon Nanotube Synthesis and Organization. In *Carbon Nanotubes: Advanced Topics in the Synthesis, Structure, Properties and Applications*, ed. A. Jorio, M. S. Dresselhaus, and G. Dresselhaus, 101-164. Springer Series in Topics in Appl. Phys. Vol. 111.

(Kroto 1985) Kroto, H. W., Heath, J. R., O'Brien, S. C., Curl, R. F., Smalley, R. E., 1985 C60: Buckminsterfullerene. *Nature* 318: 162-163

(Maciel 2008) Maciel, I. O., Anderson, N. Pimenta, M. A., Hartschuh, A., Qian, H., Terrones, M., Terrones, H., Campos-Delgado, J. Rao, A. M., Novotny, L., Jorio, A., 2008 Electron and phonon renormalization near charged defects in carbon nanotubes. *Nat. Mat.* In press.

(Mahan 2002) Mahan, G. D., 2002. Oscillations of a thin hollow cylinder: Carbon nanotubes. *Phys. Rev. B* 65: 235402.

(Malard 2008) Malard. L. M., Mafra, D. L., Guimaraes, M. H. D., Mazzoni, M. S. C., Jorio, A., 2008. Group theory analysis of optical absorption and electron scattering by phonons in mono- and multi-layer graphene. Unpublished.

(Miyata 2008) Miyata, Y., Yanagi, K., Kataura, H., 2008. Evaluation of the metal-to-semiconductor ratio of single –wall carbon nanotubes using optical absorption spectroscopy, Ninth International Conference on the science and appliactions of nanotubes, p.56, T10

(Ni 2008) Ni, Z., Wang, Y., Yu, T., You, Y., Shen, Z., 2008. Reduction of Fermi velocity in folded graphene observed by resonance Raman spectroscopy. *Phys. Rev. B* 77: 235403.

(Novoselov 2004) Novoselov, K. S., Geim, A. K., Morozov, S. V., Jiang, D., Dubonos, S. V., Girgorieva, I. V., Firsov, A. A., 2004. Electric field effect in atomically thin carbon films. *Science* 306: 666

(Novoselov 2005) Novoselov, K. S., Geim, A. K., Morozov, S. V., Jiang, D., Katsnelson, M. I., Girgorieva, I. V., Dubonos, S. V., Firsov, A. A., 2005. Two-dimensional gas of massless Dirac fermions in graphene. *Nature* 438: 197

(Oberlin 1976) Oberlin, A., Endo, M., Koyama, S., 1976. T. Filamentous growth of carbon through benzene decomposition. *J. Cryst. Growth* 32: 335.

(Pfeiffer 2008) Pfeiffer, R ., Pichler, T., Kim, Y. A., Kuzmany, H., 2008. Double-Wall Carbon Nanotubes. In *Carbon Nanotubes: Advanced Topics in the Synthesis, Structure, Properties and Applications*, ed. A. Jorio, M. S. Dresselhaus, and G. Dresselhaus, 495-530, Springer Series in Topics in Appl. Phys. Vol. 111.

(Pimenta 2007) Pimenta, M. A., Dresselhaus, G., Dresselhaus, M. S., Cançado, L. G., Jorio, A. & Saito R., 2007. Studying disorder in graphite-based systems by Raman spectroscopy. *Phys. Chem. Chem. Phys.* 9: 1276-1291.

(Piscanec 2004) Piscanec, S., Lazzeri M., Mauri, F., Ferrari, A. C., Robertson, J., 2004. Kohn Anomalies and Electron-Phonon Interactions in Graphite. *Phys. Rev. Lett.* 93: 185503.

(Radushkevich 1952) Raduchkevich, L. V. and Lukyanovich, V. M., 1952. *Zum. Fisc. Chim.,* 26: 88 (1952).

(Reich 2003) Reich, S., Thomsen, C. Maultzsch, J., 2003. Carbon Nanotubes: Basic Concepts and Physical Properties. Wiley-VCH.

(Saito 1998) Saito, R. , Dresselhaus, G. , Dresselhaus M. S., 1998 Physical Properties of Carbon Nanotubes. Imperial College Press, London.

(Saito 2003) Saito R., Gruneis, A., Samsonidze, Ge. G., Brar, V. W., Dresselhaus, G., Dresselhaus, M. S., Jorio, A., Cancado, L. G., Fantini, C., Pimenta, M. A., Souza Filho, A. G., 2003. Double resonance Raman spectroscopy of single-wall carbon nanotubes. *New J. Phys.* 5:157.1-157.15

(Samsonidze 2003) Samsonidze, Ge. G., Saito, R., Jorio, A., Pimenta, M. A., Souza Filho, A. G., Grüneis, A., Dresselhaus, G., Dresselhaus, M. S., 2003. The concept of cutting lines in carbon nanotube science. *J. Nanosc. Nanotech.* 3(6): 431-458

(Souza Filho 2007) Souza Filho, A. G., Endo, M., Muramatsu, H., Hayashi, T., Kim,Y. A., Barros, E. B., Akuzawa, N., Samsonidze, Ge. G., Saito, R., Dresselhaus, M. S., 2007. Resonance Raman scattering studies in Br_2-adsorbed double-wall carbon nanotubes. *Phys. Rev. B* 73: 235413

(Samsonidze 2004) Samsonidze, Ge. G., Chou, S. G., Santos, A. P., Brar, V. W., Dresselhaus, G., Dresselhaus, M. S., Selbst, A., Swan, A. K., Unlu, M. S., Goldberg, B. B., Chattopadhyay, D., Kim, S. N., Papadimitrakopoulos, F., 2004. Quantitative evaluation of the octadecylamine-assisted bulk separation of semiconducting and metallic single wall carbon nanotubes by resonance Raman spectroscopy. *Appl. Phys. Lett*. 85:1006-1008

(Tan 2002) Tan, P., An, L., Liu, L., Guo, Z., Czerw, R., Carroll, D. L., Ajayan. P. M., Zhang, N., Guo, H., 2002. Probing the phonon dispersion relations of graphite from the

double-resonance process of {Stokes} and anti-{Stokes} {Raman} scatterings in multiwalled carbon nanotubes. *Phys. Rev. B* 66: 245410

(Terrones 2008)) Terrones, M., Souza Filho, A. G., Rao, A. M., 2008. Doped Carbon Nanotubes: Synthesis, Characterization and Applications. In *Carbon Nanotubes: Advanced Topics in the Synthesis, Structure, Properties and Applications*, ed. A. Jorio, M. S. Dresselhaus, and G. Dresselhaus, 531-566. Springer Series in Topics in Appl. Phys. Vol. 111.

(Villalpando 2008) Villalpando-Paez, F., Son, H., Nezich, D., Hsieh, Y.P., Kong, J., Kim, Y.A., Shimamoto, D., Muramatsu, H., Endo, M., Terrones, M., Dresselhaus, M. S., 2008. Raman spectroscopy study of isolated double walled Carbon Nanotubes with different metallic and semiconducting configurations. *Nano Letters*. In press.

(Wykoff 1981) Wykoff, R. W. G., 1981. Crystal Structures. Krieger, New York. 2nd Ed.

(Zhang 2001) Zhang, Y. G., Chang, A. L., Cao, J., Wang, Q., Kim, W., Li, Y. M., Morris, N., Yenilmez, E., Kong, J., Dai, H. J., 2001. Electric-field-directed growth of aligned single-walled carbon nanotubes. *Appl. Phys. Lett.* 79: 3155–3157

(Zhang 2005) Zhang, Y., Tan, Y. W., Stormer, H. L., Kim, P., 2005. Experimental observation of the quantum Hall effect and Berry's phase in graphene. *Nature* 438: 201

Acknowledgements: M.S.D. and G.D. acknowledge NSF-DMR 07-04197. A.J. acknowledges financial support from CNPq, CAPES and FAPEMIG.